RAPID COMMUNICATIONS

PHYSICAL REVIEW E VOLUME 52, NUMBER 5 NOVEMBER 1995

Chemically frozen phase separation in an adsorbed layer

J. Verdasca, P. Borckmans, and G. Dewel

Service de Chimie-Physique/Center for Nonlinear Phenomena and Complex Systems, CP 231, Université Libre de Bruxelles, 1050-Bruxelles, Belgium

(Received 19 September 1994; revised manuscript received 5 September 1995)

A mechanism for the formation of adsorbate islands on a surface is proposed. It is based on the freezing of the phase separation in the adsorbed fluid, controlled by adsorption-desorption kinetics. The description relies on the Cahn-Hilliard equation complemented by source terms of chemical origin. In the weak segregation regime the model produces harmonic hexagonal or striped structures. Amplitude equations resulting from a weakly nonlinear approach give excellent agreement with the numerical simulations to explain the pattern competition. The high segregation regime is studied numerically producing structures of analog symmetries.

PACS number(s): 68.45.Da, 05.70.Fh, 64.60.My

There is growing experimental [1–4] and numerical [4–6] evidence of island formation in adsorbed layers. Understanding this phenomenon is of great significance since it may strongly affect the efficiency of heterogeneous catalytic reactions [2,6]. We show how the interplay between local kinetic processes and a simultaneously occurring phase transition [7,8] may provide a suitable mechanism for the formation of such frozen patterned states. In our model, we shall take into account both the kinetic exchanges between the surface and the gas bathing it, as well as the thermodynamics of phase coexistence over the surface. Below a critical temperature T_c, the lateral attractive interactions between adsorbed molecules may induce a "two-dimensional liquid-gas" transition in the chemisorbed overlayer which couples to the ongoing exchange processes.

In order to describe the kinetics of adsorption and activated desorption we introduce source terms into the mass balance equation. The time evolution of the surface coverage θ $(0<\theta<1)$ is then given by the continuity equation $\partial\theta/\partial t = Kn[\theta] - \nabla\cdot\mathbf{J}$. Here, $\mathbf{J}(\mathbf{r}) = -M\nabla\mu(\mathbf{r})$ is the mass current flow due to spatial inhomogeneities of the chemical potential where M is the surface mobility which is supposed to be constant. $Kn[\theta] = k_{\rm ad} ps(1-\theta) - k_{\rm des}\theta^2$ is the nonlinear reaction rate [9], where p is the pressure of the gas above the adsorbed layer and s the sticking coefficient. Also $k_{\rm ad}$ and $k_{\rm des}$ are, respectively, the adsorption and desorption rate constants. Assuming that spatial inhomogeneities vary slowly over the range of molecular interactions, the free energy can be cast in the usual Landau-Ginzburg form:

$$F\{\theta\} = \int d\mathbf{r}[f_L(\theta) + \kappa(\nabla\theta)^2]; \quad \mu = \frac{\delta F}{\delta\theta}.$$

The free energy $f_L(\theta)$ of the corresponding homogeneous system is taken with the usual double-well shape and $\kappa(\nabla\theta)^2$ is the first order contribution to the total free energy due to coverage gradients. In scaled variables, the resulting equation of motion takes the following form, which is an extension of the well known Cahn-Hilliard equation [10]:

$$\frac{\partial\theta}{\partial\tau} = P(1-\theta) - \theta^2 + \bar{M}\nabla^2\{a_0[(t-1)\theta^* + \tfrac{4}{3}t\theta^{*3}] - 2\kappa\nabla^2\theta\}. \tag{1}$$

The order parameter is the distance from the critical coverage $\theta^* = \theta - \theta_c = \theta - \frac{1}{2}$ and $t = T/T_c$. Also, $a_0 = 4k_B T_c$ and $\kappa = k_B T_c \xi_0^2$ where ξ_0 is a phenomenological length related to the range of the interactions. Under isothermal conditions, $P = (k_{\rm ad}s/k_{\rm des})p$— the reduced pressure of the gas phase—is the only externally tunable parameter in the model. According to its value, the dynamic exchange processes between the surface and reservoir may force the system to locally assume a coverage such that phase coexistence becomes unstable. Separation in two phases then follows [11] until a new balance between reaction and mass flow is reached. The linear dynamics of perturbations with wave number q, around the homogeneous steady state θ_S, that is the solution of $Kn[\theta_S] = 0$, is determined by the amplification factor

$$\alpha[q, \theta_S(P), P] = -h - \bar{M}\left(\frac{\partial^2 f_L}{\partial\theta^2}\right)_{\theta_S} q^2 - 2\bar{M}\kappa q^4,$$

where $h = P + 2\theta_s$ is the contribution from the reaction kinetics. At any fixed temperature below T_c, $\alpha = 0$ defines a closed instability region in the $P-q$ plane. By increasing (decreasing) P, one crosses the boundary at P_c^- (P_c^+) corresponding to an instability with wave number $(q_c^\pm)^4 = h_c^\pm/2\bar{M}\kappa$, where $h_c^\pm \equiv P_c^\pm + 2\theta_S(P_c^\pm)$. Then, as shown in Fig. 1, modulated perturbations with wave numbers within a given range will grow. One notices the appearance of a lower cut-off value q_- in the dispersion relation, due to the contribution of h. Thus, contrary to ordinary spinodal decomposition [12], soft modes are actually damped [13], meaning that the competition between adsorption and desorption acts to freeze the phase separation and prevent complete domain coarsening. The locus of the threshold points (P_c, q_c) at different temperatures defines a marginal stability curve, within the spinodal region, through the equation $t = (1 - q_c^2\xi_0^2)/(1 + 4\phi_c^2)$, where from now on $\phi_c \equiv \theta_S^*(P_c)$. As a result, the unstable region is asymmetric with respect to

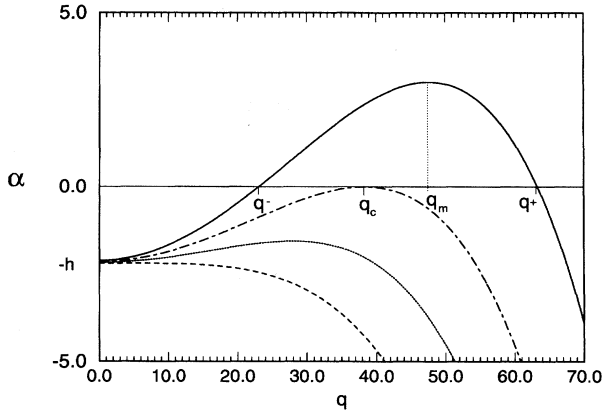

FIG. 1. Behavior of the amplification factor α as one approaches and crosses the marginal stability curve for $t=0.95$. The values are $P=0.98$, 0.96, 0.9417 (marginality), and 0.92, respectively.

$\theta_S^*=0$ but the main effect due to the chemistry is to shift t^*, the maximum temperature for the onset of the instability, below $t=1$.

We have numerically solved Eq. (1) using an explicit Euler scheme on two-dimensional square grids of size 256×256. We also performed integrations on smaller grids to ensure that finite size effects were not relevant. We fixed the temperature at $t=0.95$ and chose $\xi_0=2\times10^{-3}$, $\bar{M}a_0=\frac{1}{2}$, both sharing the units of the spatial discretization length. The initial condition was prepared by perturbing the steady state with uniformly distributed random noise. In the early stages (linear regime), the dynamics of phase separation *within* the unstable region is dominated by the most unstable mode q_m given by the linear stability analysis. The circularly averaged structure factor $S(q,\tau)$ then presents a broad peak corresponding to a wide distribution of interdroplet distances and domain sizes at early times. As domains coarsen, the peak increases in height, sharpens, and drifts towards smaller wave numbers. In this case though, it does not approach $q=0$ as it would in the absence of chemistry [12]. Instead it remains blocked at an asymptotic value q_∞ as we enter the final saturation regime where, in the case of droplet morphology, all droplets approach the same size. Later on, the system proceeds to slowly eliminate a large number of extremely robust defects generated at early times. The asymptotic state consists of hexagonally packed droplets for off-critical quenches [Figs. 2(a) and 2(c)] and interconnected, labyrinthinelike structures for near-critical quenches [Fig. 2(b)]. A completely different type of domain growth dynamics is observed *close*, but still *outside* the instability region. Droplets begin to nucleate randomly and attain their saturation radius independently of each other much faster than in the previous case. Then, ordered phase separated domains emerge from the background of linearly stable steady state coverage [Fig. 2(d)]. Finally, these domains merge and invade the whole system leading also to an extended pattern displaying hexagonal symmetry.

We found no evidence, namely in the form of dynamic scaling laws for the structure factor, for the existence of a single dominant length scale in the coarsening regime prior to saturation. Instead, multiple competitive characteristic

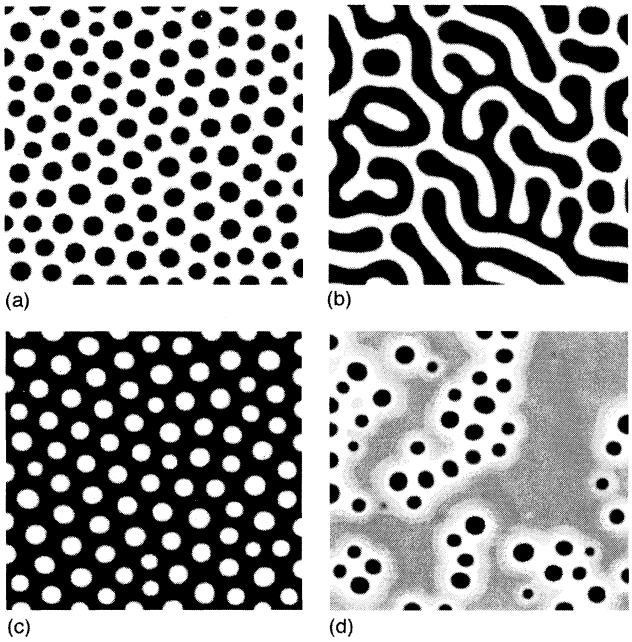

FIG. 2. (a) Quasihexagonal array of low coverage droplets at $P=0.8$ ($\theta_S^*\simeq0.08$), at late times ($\tau=246.0$). (b) Interconnected structure at $P=0.54$ ($\theta_S^*\simeq0.013$) and $\tau=170.0$. (c) Array of high coverage droplets at $P=0.4$ ($\theta_S^*\simeq-0.037$) and $\tau=250.0$. (d) Emergence of ordered domains at $P=0.96$ ($\tau=0.8$). Dark areas correspond to low coverage and light regions to high coverage. For example, in (d), black circles, white regions, and extended gray areas correspond, respectively, to coverage values of 0.3, 0.7, and 0.61 ($\simeq\theta_S$).

lengths seem to be present. Among them, two are easily identifiable and have unequivocal physical meaning: the mean droplet radius R, characterizing the average size of minority phase domains, and the average wave number defined as $\bar{q}(\tau)=\int dqqS(q,\tau)/\int dqS(q,\tau)$, which characterizes the inverse mean interdroplet distance. We followed the time evolution of the mean radius $R(\tau)$ and droplet number $N(\tau)$ by direct investigation over the grid [14]. For quenches into the instability region R and $\bar{q}$ evolve in time as displayed in Fig. 3. The dynamics slows down as time evolves and N, R, and $\bar{q}$ converge to their saturation values. Typically, saturation sets in sooner and coarsening rates are higher for deeper quenches. Also, the saturated radius R_∞ is larger for deeper quenches whereas $\bar{q}_\infty$ and N_∞ increase monotonically as the reduced pressure is increased. The fulfillment of the condition $R\sim x^{1/2}\bar{q}^{-1}$, x denoting the area fraction of minority phase, defines the crossover time from coarsening to saturation [15] and, finally, the quantity $R_\infty\bar{q}_\infty x^{-1/2}$ becomes a constant independent of the pressure. These results strongly suggest that in frozen patterns it is the difference in respective values of R that is primarily responsible for the difference in coverage at late times. Recent experiments in Langmuir films [16] show similar behavior.

The numerical results presented above were obtained in the strong segregation regime where interfaces are sharp and the amplitude saturates at values near the coexistence curve. Close to t^* there also exists a weak segregation regime where profiles are harmonic. In this limit, weakly nonlinear

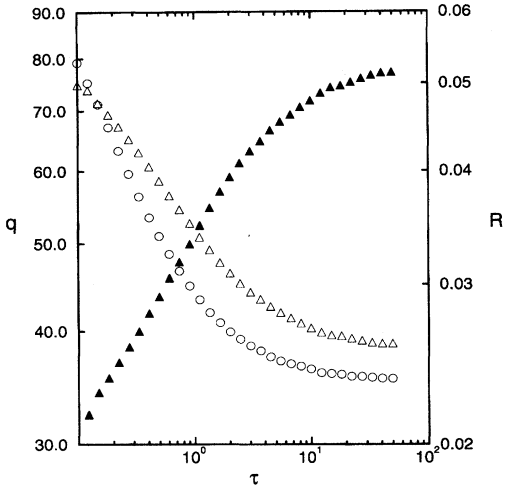

FIG. 3. Comparative time evolution of the mean droplet radius R at $P=0.8$ (▲) and the average wave number $\bar{q}$ at the same pressure (△) and at $P=0.4$ (○).

analysis may be applied to Eq. (1) to address the problem of the competition between hexagons and stripes [17]. Then, one writes the perturbations around the unstable steady state as a superposition of three excited modes: $\delta\theta \equiv \theta - \theta_S = \Sigma_{i=1}^{3} A_i e^{i(\mathbf{q}_i \cdot \mathbf{r} + \Omega_i)}$ with $|\mathbf{q}_i| = q_c$ and $\mathbf{q}_1 + \mathbf{q}_2 + \mathbf{q}_3 = \mathbf{0}$. Standard perturbative methods allow to derive a set of coupled evolution equations for the amplitudes A_i and total phase $\Omega = \Omega_1 + \Omega_2 + \Omega_3$ of the three modes, close either to the upper (+) or the lower (−) threshold:

$$\dot{A}_i = \mu^{\pm}(\phi) A_i + \nu^{\pm}(\phi) A_{i+1} \cos\Omega - g_D^{\pm} A_i^3 - g_{ND}^{\pm}(A_{i+1}^2 + A_{i-1}^2) A_i, \tag{2}$$

$$\dot{\Omega} = -\nu^{\pm}(\phi) \left(\sum_{i \neq j} A_i^2 A_j^2 / \prod_i A_i \right) \sin\Omega, \tag{3}$$

where $i=1,2,3$ and the indices are defined as modulo 3. Here, ϕ stands for $\theta_S^*(P)$ and $\phi_c^{\pm} \equiv \theta_S^*(P_c^{\pm})$. Both the linear $\mu^{\pm}(\phi) \equiv -[h - h_c^{\pm} + \Gamma_c^{\pm}(\phi^2 - \phi_c^{\pm 2})]$ and the quadratic coupling coefficient $\nu^{\pm}(\phi) \equiv -2(1 + \Gamma_c^{\pm}\phi)$ depend on the bifurcation parameter ϕ. Also $g_D^{\pm} \cong \Gamma_c^{\pm}$ and $g_{ND}^{\pm} \cong 2\Gamma_c^{\pm}$ where $\Gamma_c^{\pm} = 4\bar{M} a_0 t q_c^{\pm 2} \gg 1$. Equations (2) and (3) admit a set of steady state solutions with hexagonal symmetry ($A_i \equiv A_H$, $i=1,2,3$ and $\Omega = 0, \pi$) together with a phase invariant solution describing striped patterns ($A_1 \equiv A_S, A_2 = A_3 = 0$). Hexagonal solutions with total phase $\Omega = \pi$ ($H\pi$) are linearly stable when ν is negative, i.e., for $\phi > -(\Gamma_c^{\pm})^{-1}$. Alternatively, solutions with $\Omega = 0$ ($H0$) are only stable for $\phi < -(\Gamma_c^{\pm})^{-1}$.

Next we consider the bifurcation scenario that follows the instability at the lower threshold, ϕ_c^-. A branch of $H0$ patterns appears before the threshold with a finite amplitude (subcritical solution in the sense of bifurcation theory [17]). It extends up to the upper threshold, ϕ_c^+ [Fig. 4(a)]. On the other hand, an $H\pi$ branch bifurcates supercritically terminating abruptly at a point beyond the upper threshold. The stability limits for all hexagonal patterns, submitted to amplitude perturbations, are given by the roots of $\mu^-(\phi) = [\nu^-(\phi)]^2 (g_{ND}^- + 2g_D^-)/(g_D^- - g_{ND}^-)^2$. This equation has two real solutions $\phi = \phi_1, \phi_2$ and hexagons (both $H0$ and $H\pi$) are unstable within the range $\phi_1 < \phi < \phi_2$. So, an initially stable $H0$ branch will lose stability at $\phi = \phi_1$. However, because $\nu^-(\phi)$ changes sign between the above limits, meaning that the solution $\Omega = 0$ is no longer stable against phase perturbations, the branch subsequently stabilized at $\phi = \phi_2$ is that with the complementary phase, i.e., $H\pi$ [18]. Stripes are stable with respect to hexagons of any kind in the range between the roots of $\mu^-(\phi) = [\nu^-(\phi)]^2 g_D^-/(g_D^- - g_{ND}^-)^2$. When increasing the value of the bifurcation parameter $\phi(P)$, the following sequence of patterns emerges: the $H0$ structure is followed by stripes while the inverted hexagonal lattice, $H\pi$, appears at still higher values of ϕ until it finally relaxes to an homogeneous state. All transitions are discontinuous and by reversing the variation of the control parameter one backtracks through the various structures by undergoing hysteresis loops. A reciprocal description applies, of course, if one takes as a reference the upper threshold instead. Such a local perturbative analysis give a reliable picture of global pattern selection as long as the discrepancy between corresponding branches and stability ranges remains small. This global picture is corroborated

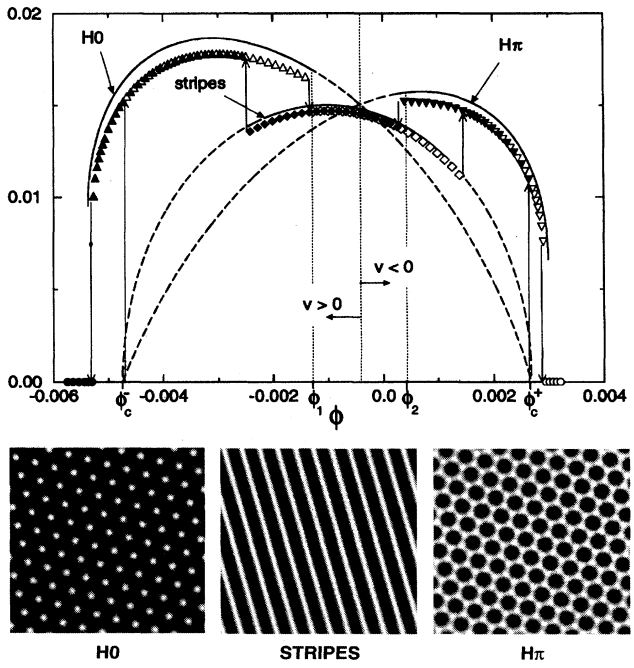

FIG. 4. (a) Amplitudes of the weakly segregated structures as a function of the bifurcation parameter ϕ at $t=0.99505$. Solid and dashed curves correspond, respectively, to stable and unstable solutions of Eqs. (2) and (3). Symbols refer to the numerical integration of Eq. (1) with the convention: ▲, △ = $H0$; ◆, ◇ = stripes; ▼, ▽ = $H\pi$; ●, ○ = homogeneous state. Empty symbols correspond to the sequence obtained by adiabatically increasing ϕ beyond ϕ_c^-. The data represented by filled symbols result when similarly decreasing ϕ below ϕ_c^+. Transitions between branches are represented by vertical arrows that delineate the hysteresis regions. (b) Modulated structures on 128×128 cellular grids. The gray scale code is the same as in Fig. 2.

by the numerical integration of Eq. (1) [Figs. 4(a) and 4(b)].

Since ϕ, which controls the sign of the quadratic term, also determines, in the strong segregation region, the nature of the (minority) droplet phase, we suggest using continuity arguments, that hexagonal arrays of high (low) coverage droplets are the extension of hexagons having total phase $0(\pi)$ in the weak segregation region. In the same vein, the structures displayed on Fig. 2(d), which appear before the marginal stability point, are evidence for a subcritical bifurcation even in the strong segregation regime. Moreover, droplet growth dynamics is substantially different for quenches into the linearly unstable supercritical and in the subcritical region. In the latter there is a total suppression of the ripening process through evaporation-condensation and/or collision-coalescence mechanisms.

In conclusion, the present model describes some processes of island formation on catalytic surfaces. We summarize the mechanism in the following way: the exchanges between surface and the gas tend to homogenize the spatial distribution of adsorbed molecules. Since adsorption (desorption) will preferentially take place in regions where coverage is lower (higher), the kinetics tends to mix the phases. Therefore, long distance correlations are introduced in the system and compete with the short-range attractions responsible for the phase transition. These correlations seem to play the same role (namely by slowing down the coarsening selecting a finite wavelength and hexagonal or stripe symmetries) as long-range repulsive interactions [19] in systems such as uniaxial ferromagnetic films [20], monomolecular organic films and lipid monolayers [16,21]. The mesoscopic nature of domain size is consistent with experimental evidence that chemisorbed molecules are organized in relatively small clusters with average sizes ranging from a few hundreds to a few thousand particles [1,3].

We thank Professor G. Nicolis for his interest in this work and H. Scheepers for providing useful numerical tools. J.V. was financially supported by JNICT (Portugal) under program CIENCIA (Grant No. BD-2004/92-RM). P.B. and G.D. were supported by F.N.R.S. (Belgium). This work was supported by the EC Science Program Grant No. (SCI-CT91-0706).

[1] T. Engel and G. Ertl, J. Chem. Phys. **69**, 1267 (1978); Adv. Catal. **28**, 1 (1979).

[2] J. L. Gland and E. B. Kollin, J. Chem. Phys. **78**, 963 (1983); G.-C. Wang and T.-M. Lu, Phys. Rev. Lett. **50**, 2014 (1983).

[3] E. D. Williams, W. H. Weinberg, and A. C. Sobrero, J. Chem. Phys. **76**, 1150 (1982).

[4] R. A. Schmitz, G. A. D'Netto, L. F. Razon, and J. R. Brown, in *Chemical Instabilities*, edited by G. Nicolis and F. Baras (Reidel, Dordrecht, 1984), p. 33.

[5] M. Stiles and H. Metiu, Chem. Phys. Lett. **128**, 337 (1986).

[6] M. Silverberg, A. Ben-Shaul, and F. Rebentrost, J. Chem. Phys. **83**, 6501 (1985).

[7] B. A. Huberman, J. Chem. Phys. **65**, 2013 (1976); E. Coutsias and B. A. Huberman, Phys. Rev. B **24**, 2592 (1981).

[8] G. Ertl, Science **254**, 1750 (1991) and references therein.

[9] It can also be regarded as a single component autocatalytic reaction.

[10] J. W. Cahn and J. E. Hilliard, J. Chem. Phys. **28**, 558 (1958); **31**, 688 (1959).

[11] For a review on phase separation dynamics, see J. D. Gunton, M. San Miguel, and P. Sahni, in *Phase Transitions and Critical Phenomena*, edited by C. Domb and J. Lebowitz (Academic, New York, 1983), Vol. 8.

[12] J. S. Langer, M. Bar-on, and H. O. Miller, Phys. Rev. A **11**, 1417 (1975). See also the review article by J. S. Langer, in *Solids Far From Equilibrium*, edited by C. Godrèche (Cambridge University Press, Cambridge, 1992), p. 297.

[13] S. C. Glotzer, E. A. Di Marzio, and M. Muthukumar, Phys. Rev. Lett. **74**, 2004 (1995).

[14] We have binarized the grid and evaluated the total number and area of closed domains, that become circular early in the evolution. This method makes our data for R directly comparable to modern video-monitored experiments proceeding via direct-imaging techniques.

[15] M. Seul, N. Morgan, and C. Sire, Phys. Rev. Lett. **73**, 2284 (1994).

[16] N. Morgan and M. Seul, J. Phys. Chem. **99**, 2088 (1995).

[17] P. Borckmans, G. Dewel, A. De Wit, and D. Walgraef, in *Chemical Waves and Patterns*, edited by R. Kapral and K. Showalter (Kluwer, Dordrecht, 1995), p. 323; M. C. Cross and P. C. Hohenberg, Rev. Mod. Phys. **65**, 851 (1993).

[18] J. Verdasca, A. De Wit, G. Dewel, and P. Borckmans, Phys. Lett. A **168**, 194 (1992).

[19] C. Roland and R. C. Desai, Phys. Rev. B **42**, 6658 (1990).

[20] M. Seul and C. A. Murray, Science **262**, 558 (1993); C. Sagui and R. Desai, Phys. Rev. E **49**, 2225 (1994).

[21] C. M. Knobler and R. C. Desai, Annu. Rev. Phys. Chem. **43**, 207 (1992).

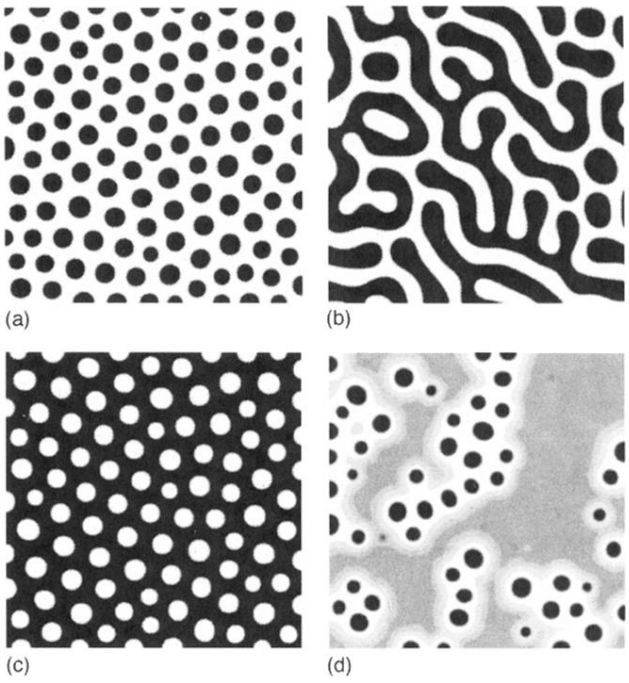

FIG. 2. (a) Quasihexagonal array of low coverage droplets at $P=0.8$ ($\theta_S^* \simeq 0.08$), at late times ($\tau=246.0$). (b) Interconnected structure at $P=0.54$ ($\theta_S^* \simeq 0.013$) and $\tau=170.0$. (c) Array of high coverage droplets at $P=0.4$ ($\theta_S^* \simeq -0.037$) and $\tau=250.0$. (d) Emergence of ordered domains at $P=0.96$ ($\tau=0.8$). Dark areas correspond to low coverage and light regions to high coverage. For example, in (d), black circles, white regions, and extended gray areas correspond, respectively, to coverage values of 0.3, 0.7, and 0.61 ($\simeq \theta_S$).

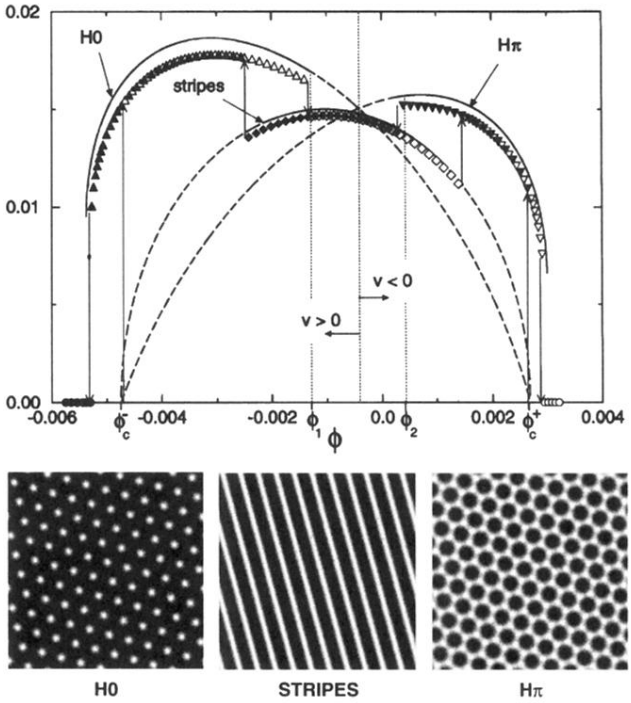

FIG. 4. (a) Amplitudes of the weakly segregated structures as a function of the bifurcation parameter ϕ at $t=0.99505$. Solid and dashed curves correspond, respectively, to stable and unstable solutions of Eqs. (2) and (3). Symbols refer to the numerical integration of Eq. (1) with the convention: ▲, $\triangle = H0$; ◆, ◇ = stripes; ▼, $\nabla = H\pi$; ●, ○= homogeneous state. Empty symbols correspond to the sequence obtained by adiabatically increasing ϕ beyond ϕ_c^-. The data represented by filled symbols result when similarly decreasing ϕ below ϕ_c^+. Transitions between branches are represented by vertical arrows that delineate the hysteresis regions. (b) Modulated structures on 128×128 cellular grids. The gray scale code is the same as in Fig. 2.